Characterization of an Intraluminal Differential Frequency-Domain Photoacoustics System

Bahman Lashkari[a], Jungik Son[b], Simon Liang [a], Robin Castelino[b],
F. Stuart Foster[b], Brian Courtney[c], Andreas Mandelis*[a]
[a]Center for Advanced Diffusion-Wave Technologies (CADIFT), Department of Mechanical and Industrial Engineering, University of Toronto, Toronto, M5S 3G8, Canada; [b]Sunnybrook Research Institute, Toronto, M4N 3M5, Canada; [c]Conavi Medical Inc., Toronto, Canada

ABSTRACT

Cardiovascular related diseases are ranked as the second highest cause of death in Canada. Among the most important cardiovascular diseases is atherosclerosis. Current methods of diagnosis of atherosclerosis consist of angiography, intravascular ultrasound (IVUS) and optical coherence tomography (OCT). None of these methods possesses adequate sensitivity, as the ideal technique should be capable of both depth profiling, as well as functional imaging. An alternative technique is photoacoustics (PA) which can perform deep imaging and spectroscopy. The presented study explores the application of wavelength-modulated differential photoacoustic radar (WM-DPAR) for characterizing arterial vessels. The wavelength-modulated differential photoacoustic technique was shown to be able to substantially increase the dynamic range and sensitivity of hemoglobin oxygenation level detection. In this work the differential PA technique was used with a very high frequency modulation range. To perform spectroscopic PA imaging, at least two wavelengths are required. The selected wavelengths for this work are 1210 nm and 980 nm. 1210 nm corresponds to the maximum optical absorption coefficient of cholesterol and cholesteryl esters which are the main constituents of plaques. Since water, elastin and collagen also have high absorption coefficients at 1210 nm, this wavelength alone cannot provide very high sensitivity and specificity. The additional wavelength, 980 nm corresponds to high absorption coefficient of those constituents of healthy artery tissue. The simultaneous application of the abovementioned wavelengths can provide higher sensitivity and improved specificity in detecting lipids in the arterial vessels.

Keywords: Intravascular photoacoustic imaging, photoacoustic endoscopy, photoacoustic spectroscopy, frequency-domain photoacoustics, waveform engineering.

1. INTRODUCTION

According to Statistics Canada, in the year 2012, 61,855 deaths were recorded due to cardiovascular related diseases. This accounts for 25% of the total number of deaths in Canada in that year. Among the most important cardiovascular diseases is atherosclerosis, a chronic disease occurring with gradual build-up of lipid rich plaques in the inner layer of the arterial wall. Angiography, intravascular ultrasound (IVUS) and optical coherence tomography (OCT) are currently employed by clinicians for diagnosis of atherosclerosis. None of these methods is capable of both depth profiling and functional imaging. Photoacoustic (PA) imaging is an emerging technology for intravascular imaging and characterization.[2-11] The spectroscopic and deep imaging capabilities of PA makes it an ideal candidate for diagnosis of atherosclerosis. Furthermore, since plaques are located superficially, optical scattering is minimal. Therefore, PA functional imaging faces fewer challenges than the case of deep targets.[12] Diagnosis of atherosclerosis by PA is mainly based on detection of lipids in the arterial wall. Allen et al.[7] focused on some of the important constituents of healthy arterial walls and plaques in the 740 to 1400 nm wavelength range. To isolate the plaque boundary and enhance the specificity of lipid-rich plaque detection, they employed two wavelengths; 1210 nm and 980 nm.

*mandelis@mie.utoronto.ca; phone 1 416 978-1287; fax 1 416 978-6061; mie.utoronto.ca

Photons Plus Ultrasound: Imaging and Sensing 2016, edited by Alexander A. Oraevsky, Lihong V. Wang
Proc. of SPIE Vol. 9708, 970808 · © 2016 SPIE · CCC code: 1605-7422/16/$18 · doi: 10.1117/12.2214152

The first wavelength, 1210 nm, is located at the lipid absorption peak. Since the main components of a healthy arterial wall (mainly water, elastin and collagen) have a high absorption coefficient at 1210 nm, the second wavelength is also required. Water, elastin and collagen have strong optical absorption at 980 nm, while, the lipid optical absorption coefficient is weak at this wavelength. By using difference imaging at the abovementioned wavelengths, they showed the possibility of detecting fatty plaques with high specificity. The present paper is based on the real-time application of a similar idea. We demonstrate that simultaneous emission of two out-of-phase continuous-wave (CW) lasers makes it possible to enhance the specificity, sensitivity and speed of imaging.

CW intensity-modulated laser PA has some unique capabilities. The phase in the frequency-domain (FD) PA provides an extra channel that facilitates imaging and probing. It can be used to enhance the image resolution and contrast.[13,14] Phase can also provide a calibration-free technique for functional imaging.[15] Another unique capability of FD-PA is simultaneous multi-wavelength irradiation that enhances the speed of probing and imaging.[16] Wavelength-modulated differential PA is a technique that has been employed for detection of oxygen saturation level of hemoglobin and was shown to be capable of increase in detection sensitivity and dynamic range.[17,18] The presented study extends the application of wavelength-modulated differential PA to endoscopy. We employed two simultaneous out-of-phase linear frequency modulation chirps to distinguish lipids.

2. THEORETICAL BACKGROUND OF DIFFERENTIAL FREQUENCY-DOMAIN PHOTOACOUSTIC SPECTROSCOPY

To enhance the specificity of atherosclerosis diagnosis by differential FD-PA, the PA signal should be able to differentiate between normal tissue (background) and fatty plaque. This can be performed by employing two lasers with proper wavelengths. The idea is to simultaneously transmit two intensity-modulated chirps with identical sweep frequencies while there is a constant phase difference of approximately π between the waveforms. These two lasers with specific wavelengths are employed simultaneously to induce PA signals on one chromophore. The wavelengths are chosen in a way that the two PA signals cancel each other out for the case of healthy tissue. However, if tissue consists of lipids, due the high absorption coefficient at one wavelength and low absorption coefficient at the other wavelength, a strong signal is generated. The two abovementioned wavelengths of 980 nm and 1210 nm are chosen for this application. The absorption coefficient spectra of main constituents of healthy tissue; water, elastin and gelatin versus lipids shows the rationale for selecting these wavelengths. All of the main components of healthy tissue have very similar absorption coefficients at 980 nm and 1210 nm. It helps to eliminate the PA signal from these components and generate a zero baseline. On the other hand, lipids, cholesterol and cholesteryl esters in particular, have a very high absorption coefficient at 1210 nm and a very low absorption at 980 nm. Based on these facts we can develop an analytical formulation for this problem. The two linear frequency modulation (LFM) chirps can be described as follows:

$$I_1(t) = A_1\left[1+\sin(\omega_c t+\frac{\pi B_{ch}}{T_{ch}}t^2)\right], \qquad -\frac{T_{ch}}{2}<t<\frac{T_{ch}}{2}, \tag{1}$$

$$I_2(t) = A_2\left[1+\sin(\omega_c t+\frac{\pi B_{ch}}{T_{ch}}t^2+\varphi)\right], \qquad -\frac{T_{ch}}{2}<t<\frac{T_{ch}}{2}, \tag{2}$$

where I_1 and I_2 are the intensities of the two lasers, and A_1 and A_2 are the corresponding amplitudes. T_{ch} is the chirp duration, B_{ch} is the chirp bandwidth, ω_c is the mean angular frequency of the chirp and, φ is the phase difference between the two chirp waveforms. The cross-correlation signal based on 1D solution for one of the wavelengths is (Fig.1):[19]

$$R_1(t) \approx \eta\left(\frac{T_{ch}}{4B_{ch}}\right)\int_{f_1}^{f_2}\frac{\Gamma A_1 e^{-\mu_{eff1}L_1}\mu_{a1}}{\mu_{a1}c+j\omega}e^{j\omega(t-\frac{L}{c})}\tilde{H}_{tr}(f)\,df \tag{3}$$

where f_1 and f_2 are the starting and ending frequencies of the chirp, respectively, Γ is the Grüneisen parameter, H_{tr} and η are the transfer function and sensitivity of the ultrasonic transducer, respectively; c is the speed of sound in the tissue; μ_{a1} is the absorption coefficient of the component at wavelength #1; μ_{eff1} is the effective optical attenuation coefficient of the overlying tissue at laser wavelength #1; L_1 is the thickness of the scattering overlayer medium; L is the distance of the transducer from the absorber surface. Since atherosclerotic plaque is located within a very shallow depth underneath the surface (L_1 is very small), the optical attenuation term can be ignored. It should be added that due to the very high

Grüneisen parameter value of lipids as well as its different behavior with temperature change, this parameter can have a very significant effect on the contrast and sensitivity of intravascular PA imaging.[12,20]
It can be shown that the response of a linear causal system, to the Hilbert transform of an excitation input signal is equal to the Hilbert transform of the system response to that input signal. We use this property to superpose the PA response of the two lasers. Therefore, the cross-correlation of the detected signals stimulated by the abovementioned LFM chirps in Eqs. (1) and (2) can be approximated as:

$$R(t) \approx \eta\left(\frac{T_{ch}\Gamma}{4B_{ch}}\right)\int_{f_1}^{f_2}\left[\left[\left(\frac{A_1\mu_{a1}}{\mu_{a1}c+j\omega}\right)+\left(\frac{A_2\mu_{a2}e^{-j\varphi}}{\mu_{a2}c+j\omega}\right)\right]e^{j\omega(t-\frac{L}{c})}\tilde{H}_{tr}(f)\,df\right] \tag{4}$$

where μ_{a2} is the absorption coefficient of the chromophore at the second employed wavelength. In the case of the background tissue (water, elastin, or collagen) the differential PA cross-correlation signal must become zero. This is possible only if $A_1\mu_{a1} = A_2\mu_{a2}$ (condition 1). Additionally, it is required to have a proper phase difference between the two signals. Some simplifying assumptions can be used to estimate the required phase difference. We ignore the effect of the transducer transfer function ($H_{tr}(f)$=1 for $f_1<f<f_2$) and also assume: $c\mu_{a1\,or\,2} << \omega$. Therefore, it can be shown that the phase difference should approximately be:

$$\varphi \approx \pi + \tan^{-1}\left\{\frac{2\pi f_1 f_2 B_{ch}\ln\left(f_1/f_2\right)c\left(\mu_{a2}-\mu_{a1}\right)}{\left(2\pi f_1 f_2\ln\left(f_1/f_2\right)\right)^2 + B_{ch}c^2\left(\mu_{a2}\mu_{a1}\right)}\right\} \qquad \text{(condition 2)}$$

Condition 2, shows that if $\mu_{a1}=\mu_{a2}$, then the phase difference between the two chirps should be π. Furthermore, simple calculations show that in the high frequency range (e.g. 12-17 MHz), the second term is very small and therefore, $\varphi \approx \pi$

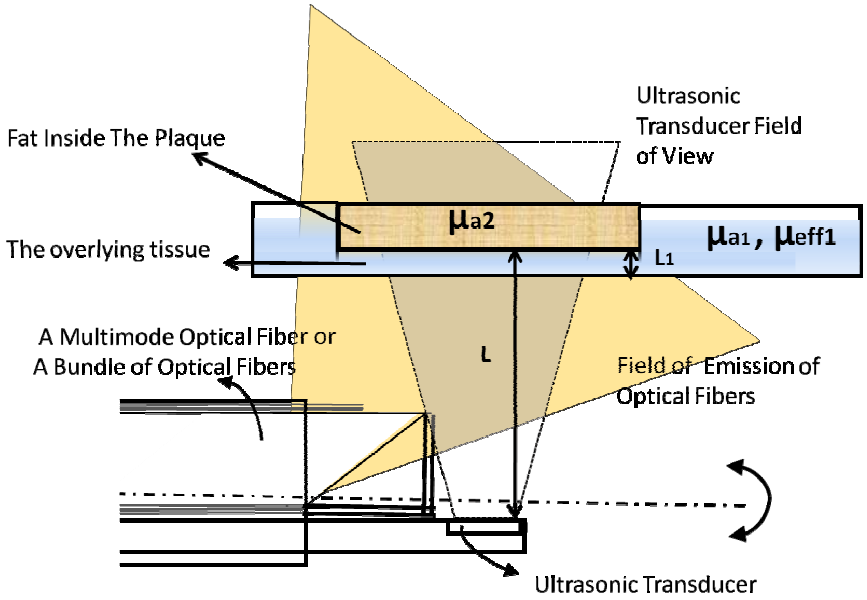

Figure 1. A simplified model of intravascular PA atherosclerosis detection.

3. EXPERIMENTAL SET-UP

A schematic diagram of the experimental set-up is shown in Fig. 2. The experimental set-up consisted of two laser diodes, 980 nm and 1210 nm (LDX Optronics Inc., Maryville, TN, USA). The diodes were modulated by two identical high-frequency drivers VFM10-25 (MESSTEC Power Converter GmbH, Germany), where these drivers received their input from a dual-channel arbitrary waveform generator (33500B, Agilent Technologies, Inc. Loveland, CO, USA). The

temperature of the laser diodes was stabilized at 23°C employing two thermo-electric controllers (Arroyo Inst. 5305, San Luis, CA, USA). The laser fluences were combined using a fiber multiplexer (WDM-12P-111-980/1210-400/440-QMQMQM-35-555-3A-1, OZ Optics, Ottawa, ON, Canada). Two ultrasonic transducers were used for this work: one was a 10-MHz device (8865 A101, Imasonic, France) and the second one was a 1.5 mm x1.5 mm, 14-MHz piezoelement (Sunnybrook Research Institute, Toronto, Canada). The output signal of the transducers was amplified (preamplifier model 5676, Panametrics, Olympus, USA) and then digitized using a data acquisition card (NI PXIe 5122, TX, USA). The artery phantom was located on a rotating stage and the lumen was filled with electrode gel for acoustic coupling. The signal processing and image reconstruction were performed using the NI controller system (NI PXIe-8135, NI, TX, USA). As shown in Fig. 1, the goal is to join the optical fiber and the peizoelement together, however, at this stage the experiments were performed with PA signals in the forward mode (Fig. 2). In the future experiments, the catheter will include both piezoelement and the optical fiber.

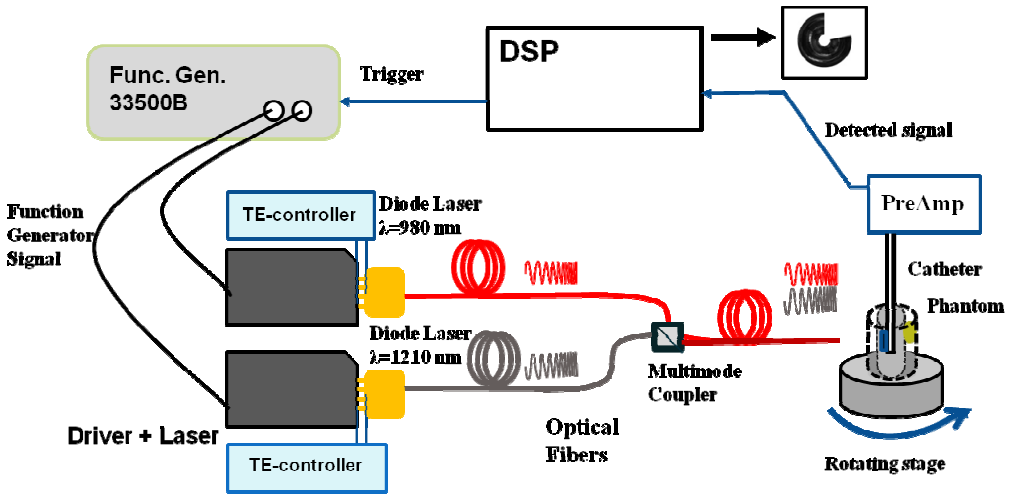

Figure 2. Experimental set-up.

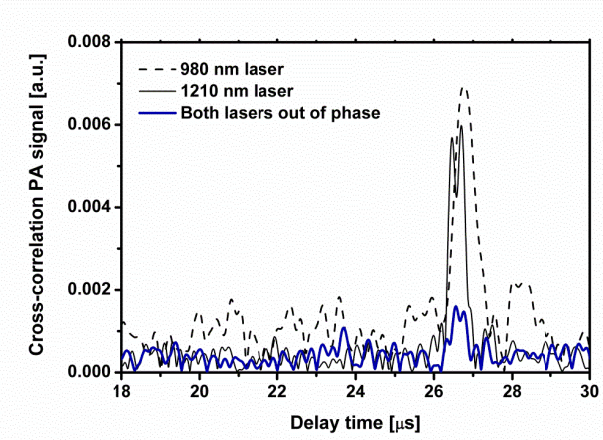

Figure 3. PA signals with both lasers emitting individually and the differential PA signal. The phantom was a PVC-Plastisol sample and a 10-MHz transducer was employed with two chirps sweeping from 4 MHz to 10 MHz.

4. EXPERIMENTAL RESULTS

One experiment was performed on PVC-plastisol sample. The aim of this experiment was to demonstrate the possibility of suppressing the signal by out of phase emissions of two lasers. The 10-MHz transducer was employed and chip frequencies sweeps were from 4 to 10 MHz. Figure 3 shows the individual PA signals using the two lasers. Additionally, the differential wavelength-modulated PA signal is also shown. The laser intensities were adjusted by changing the

amplitude in the function generator. It can be observed that by emitting both lasers simultaneously, but with 180° phase difference, it is possible to minimize the output signal.

In another experiment a gelatin phantom was made to simulate an arterial vessel. On one side of the vessel a dent was generated and filled with a cholesterol oleate lump (Alf Aesar, Ward Hill, MA, USA). The sample was located on a rotating stage and imaged 28 times with 10° rotation in each step. The 14-MHz ultrasound catheter was located in the phantom lumen with the piezoelement facing the output of laser fiber. The frequency range of 6-12 MHz was used, once with 1210 nm laser alone and again with both lasers (out of phase) on. The images are shown in Figs. 4(a) and (b). In Fig. 4(a), the image shows the cholesterol oleate lump area, but the surface of the gelatin around the phantom can also be seen. Figure 4(b) however, only shows the cholesterol oleate lump. It is interesting to note that in the lower part of Fig. 4(a), the gelatin generated a strong signal that can be mistaken for a fatty deposit. The fact that this spot does not appear in the differential image shows the higher specificity of differential FD-PA imaging.

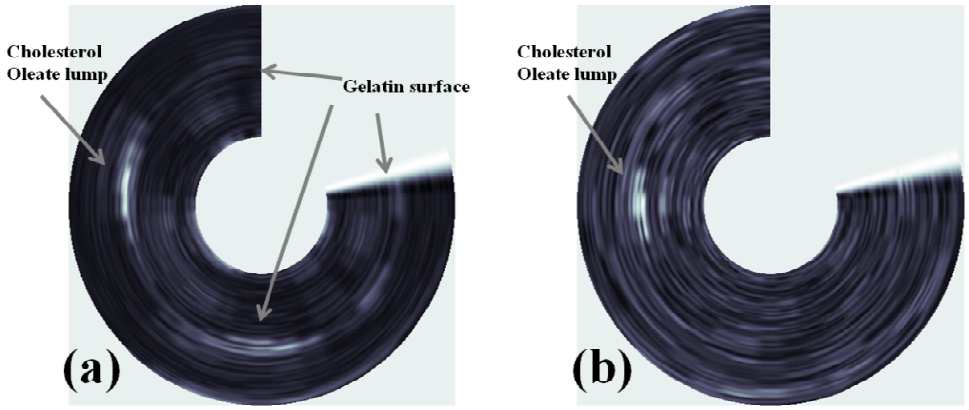

Figure 4. Images of artery phantom with a cholesterol oleate lump in one side generated by (a) FD-PA with 1210 nm laser, (b) differential FD-PA employing 1210 and 980 nm lasers with out-of-phase chirps.

5. SUMMARY

Among the most important cardiovascular diseases is atherosclerosis. Current methods of diagnosis of atherosclerosis do not provide adequate sensitivity. Photoacoustics (PA) is an alternative technique capable of deep subsurface spectroscopic imaging. The presented study explores the application of differential FD-PA for the diagnosis of atherosclerosis. To perform spectroscopic PA imaging two wavelengths, 1210 and 980 nm, were employed. 1210 nm corresponds to the maximum optical absorption of cholesterol and cholesteryl esters which are the main constituent of plaque. The other wavelength corresponds to high optical absorption of constituents of healthy artery tissue. It was shown that differential FD-PA can provide higher specificity in detecting lipids in the arterial vessels by efficiently suppressing contributions of non-fatty tissue to the PA image.

ACKNOWLEDGMENT

The support of an NSERC-CIHR CHRP grant to A. Mandelis and F.S. Foster and of the Canada Research Chairs program to A. Mandelis is gratefully acknowledged.

REFERENCES

[1] Statistics Canada, "Leading causes of death," 10 December 2015, http://www.statcan.gc.ca/tables-tableaux/sum-som/l01/cst01/hlth36a-eng.htm (15 January 2016).

[2] Sethuraman, S., Aglyamov, S. R., Amirian, J. H., Smalling, R. W., and Emelianov, S. Y., "Intravascular photoacoustic imaging using an IVUS imaging catheter," IEEE Trans. Ultrason. Ferroelectr. Freq. Control 54(5), 978–986 (2007).

[3] Sethuraman S., Amirian, J. H., Litovsky S. H., Smalling R. W., and Emelianov S. Y., "Spectroscopic intravascular photoacoustic imaging to differentiate atherosclerotic plaques," Opt Express 16, 3362–3367 (2008).
[4] Karpiouk, A. B., Wang, B., and Emelianov, S. Y., "Development of a catheter for combined intravascular ultrasound and photoacoustic imaging," Rev. Sci. Instrum. 81, 014901 (2010).
[5] Wang, B., Karpiouk, A., Yeager, D., Amirian, J., Litovsky, S., Smalling, R., Emelianov, S., "In vivo intravascular ultrasound-guided photoacoustic imaging of lipid in plaques using an animal model of atherosclerosis," Ultrasound Med. Biol. 38, 2098–2103 (2012).
[6] Wang, B., Karpiouk, A., Yeager, D., Amirian, J., Litovsky, S., Smalling, R., Emelianov, S., "Intravascular photoacoustic imaging of lipid in atherosclerotic plaques in the presence of luminal blood," Opt. Lett. 37, 1244–1246 (2012).
[7] Allen, T. J., Hall, A., Dhillon, A. P., Owen J. S., and Beard, P. C., "Spectroscopic photoacoustic imaging of lipid-rich plaques in the human aorta in the 740 to 1400 nm wavelength range," J. Biomed. Opt. 17(6), 0612209 (2012).
[8] Jansen, K., Wu, M., van der Steen, A. F. W., and van Soest, G., "Photoacoustic imaging of human coronary atherosclerosis in two spectral bands," Photoacoustics 2(1), 12–20 (2014).
[9] Jansen, K., van der Steen, A. F., Wu, M., van Beusekom, H. M., Springeling, G., Li, X., Zhou, Q., Shung, K. K., De Kleijn, D. P., and van Soest, G., "Spectroscopic intravascular photoacoustic imaging of lipids in atherosclerosis," J. Biomed. Opt. 19(2), 026006 (2014).
[10] Li, X., Wei, W., Zhou, Q., Shung, K. K., Chen, Z., "Intravascular photoacoustic imaging at 35 and 80 MHz," J. Biomed. Opt. 17, 106005 (2012).
[11] Abran, M., Cloutier, G., Cardinal, M.-H.R., Chayer, B., Tardif, J.-C., Lesage, F., "Development of a Photoacoustic, Ultrasound and Fluorescence Imaging Catheter for the Study of Atherosclerotic Plaque," IEEE Trans. Biomed. Circuits Syst. 8(5), 696-703 (2014).
[12] Cox, B., Laufer, J.G., Arridge, S.R., and Beard, P.C., "Quantitative spectroscopic photoacoustic imaging: a review," J. Biomed. Opt. 17(6), 061202 (2012).
[13] Lashkari, B., and Mandelis, A., "Comparison between pulsed laser and frequency-domain photoacoustic modalities: signal-to-noise ratio, contrast, resolution, and maximum depth detectivity," Rev. Sci. Instrum. 82(2), 1324 (2011).
[14] Dovlo, E., Lashkari, B., Mandelis, A., Shi, W., and Liu, F.-F., "Photoacoustic radar phase-filtered spatial resolution and co-registered ultrasound image enhancement for tumor detection," Biomed. Opt. Express 6(3), 1003-1009 (2015).
[15] Lashkari, B., Choi, S.S., Dovlo, E., Dhody, S., and Mandelis, A., "Frequency-domain photoacoustic phase spectroscopy: A fluence-independent approach for quantitative probing of hemoglobin oxygen saturation," IEEE J. Sel. Top. Quantum Electron. 22(3), (DOI 10.1109/JSTQE.2015.2494532) (2016).
[16] Lashkari, B., Choi, S.S., Khosroshahi, M.E., Dovlo, E., Mandelis, A., "Simultaneous dual-wavelength photoacoustic radar imaging using waveform engineering with mismatched frequency modulated excitation," Opt. Lett. 40(7), 1145-1148 (2015).
[17] Choi, S.S., Mandelis, A., Guo, X., Lashkari, B., Kellnberger, S., and Ntziachristos, V., "Wavelength-Modulated Differential Photoacoustic Spectroscopy (WM-DPAS): Theory of a High-Sensitivity Methodology for the Detection of Early-Stage Tumors in Tissues," Int. J. Thermophys. 36, 1305–1311 (2015).
[18] Choi, S.S., Mandelis, A., Guo, X., Lashkari, B., Kellnberger, S., and Ntziachristos, V., "Wavelength-modulated differential photoacoustic spectroscopy (WM-DPAS) for noninvasive early cancer detection and tissue hypoxia monitoring," J. Biophotonics 1-8, DOI 10.1002/jbio.201500131 (2015).
[19] Lashkari, B., and Mandelis, A., "Linear Frequency Modulation Photoacoustic Radar: Optimal Bandwidth for Frequency-domain Imaging of Turbid Media," J. Acoust. Soc. Am. 130(3), 1313-1324 (2011).
[20] Wang, B., Emelianov, S., "Thermal intervascular photoacoustic imaging," Biomed. Opt. Express 2(11), 3072-3078 (2011).